Supplemental material for

Néel-type skyrmion lattice in tetragonal polar magnet $VOSe_2O_5$

Takashi Kurumaji[1]*, Taro Nakajima[1], Victor Ukleev[1], Artem Feoktystov[2],

Taka-hisa Arima[1,3], Kazuhisa Kakurai[1,4], and Yoshinori. Tokura[1,5]

1. **Single crystal growth and magnetization measurement with assembled single crystals.**
2. **SANS investigation with a magnetic field along the *a* axis.**

1. Single crystal growth and magnetization measurement with assembled single crystals.

Single crystals of $VOSe_2O_5$ were grown by the chemical vapor transport reaction. Sizes of the obtained single crystals were typically 0.5 × 0.5 × 0.7 mm^3. First, powder of $VOSe_2O_5$ was synthesized by the solid-state reaction as described in Ref. [17,19]. Next, we charged the powder of $VOSe_2O_5$ (0.5 g) with the transport agent NH_4Cl (around 30 mg) at an end of the sealed quartz tube (length: 120 mm, diameter: 18 mm), and placed this tube in a three-zone furnace with the temperature gradient from 400 ^oC to 350 ^oC. The duration for the main transport process is typically two months. We introduced a pre-reaction process with the temperature 380 ^oC on the source side for around four days in order to induce the partial decomposition reaction: $VOSe_2O_5 \rightarrow VOSeO_3 + SeO_2$, which is important to eliminate the production of VO_2 on the source side, as VO_2 is detrimental for the formation of $VOSe_2O_5$ as the final product.

Figure S1(a) shows the photograph of the co-aligned single crystals for the SANS measurements. Each sample has clear crystallographic facets typically for (001), (100), and (110) planes. The co-alignment was performed by putting the samples on the flat aluminum plate, and attaching a facet on one crystal with that of the other, for example, one's (100) plane with the other's (-100) plane (see Fig. S1(b)). For the in-plane orientation, we performed the single crystal x-ray diffraction for each sample in order to distinguish (100) planes from (110) planes.

The demagnetization field for the co-aligned sample shifts the magnetic phases towards higher field than those of the single piece of a crystal. We performed the

measurement of magnetic properties for the assembled sample as shown in Figs. S1(c)-S1(f)). Figure S1(c) shows the temperature dependence of χ' in zero field with the ac magnetic field (H_{ac}) along the *c* axis. The onset of the cycloidal spin state (IC-1) is clearly discerned by a peak at 7.50 K, and the transition to the B phase is also observed as indicated by a black triangle. These clear phase transitions indicate the homogeneous high quality of each single crystal for the SANS measurement. Figure S1(d) shows the behavior of χ' around T_C under $H//c$. For H = 20 Oe ~ 30 Oe, a dip structure is observed, indicating the triangular SkL state. The SkL state is also confirmed in the H dependence of χ' as shown in Fig. S1(e). Clear double-peak structure is observed at 7.45 K. This feature is slightly broadened as decreasing temperature due perhaps to the inhomogeneous demagnetization field. This may be the reason for the multidomain state in terms of the triangular SkL, IC-1, and IC-2 states as seen in Fig. 3(a). As indicated by a black triangle in Fig. S1(e), shoulder structure is discernible. We assigned it to the phase boundaries for the triangular SkL state against the IC-1 phase and FM phase with spins parallel to the *c* axis. Figure S1(f) is the *H*-*T* phase diagram with $H//c$ determined by the magnetization measurements with the assembled-crystals sample. The magnetic fields for the phase boundaries are shifted towards high field due to the demagnetization field, but the clear pocket-like region for the triangular SkL state is identified.

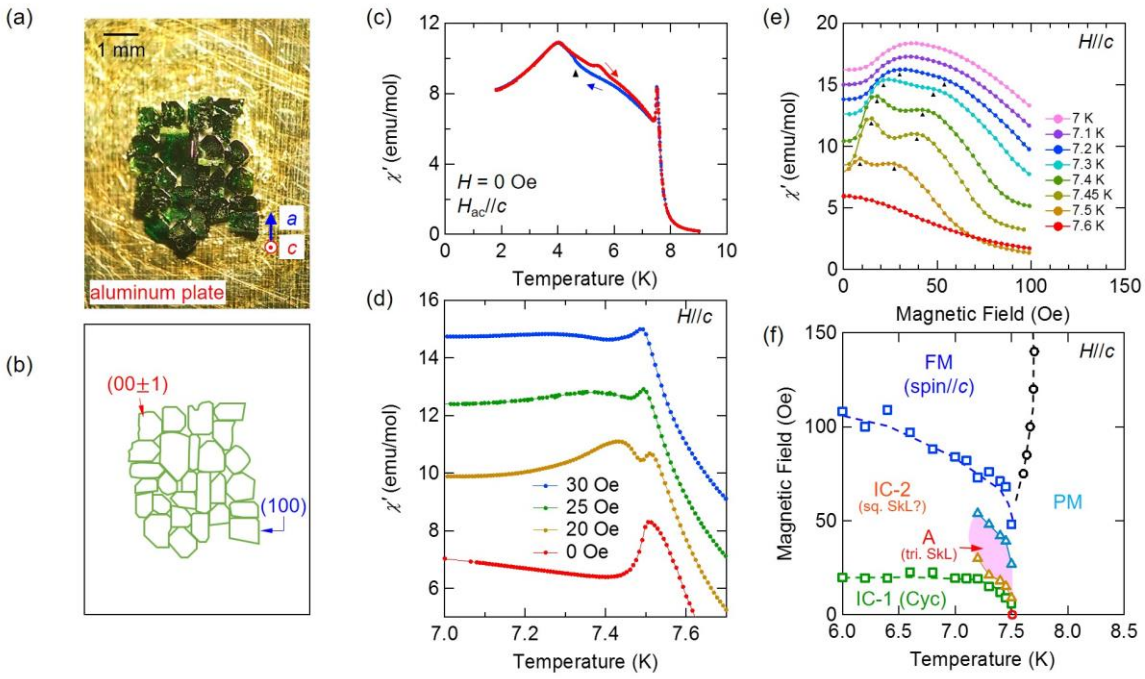

FIG. S1. (a) Photograph of the sample for the SANS measurement. Twenty-seven pieces of single crystals are assembled to be co-aligned with the *a* and *c* axes. (b) Outline of each single crystal. (c-e) The real part of the ac magnetic susceptibility χ' data for the assembled single crystals. (c) Temperature dependence of χ' in zero field. Black triangle indicates the anomaly for the transition from IC-1 phase to the B phase in the cooling process. (d,e) Temperature and *H* dependence of χ' with *H*//*c*, respectively. Data are shifted vertically for clarity. In (e), black triangles indicate the peak or shoulder structures of χ', assigned to the phase boundary between triangular SkL state and IC-1/FM state. (f) *H*-*T* phase diagram under *H*//*c* for the assembled single crystals determined by the magnetization measurements.

2. SANS investigation with a magnetic field along the *a* axis

SANS measurements were performed using the instrument KWS-1 of Jülich Centre for Neutron Science (JCNS) at Heinz Maier-Leibnitz Zentrum (MLZ), Garching, Germany [21,22]. The neutron beam was collimated over a length of 20 m before reaching the sample. The scattered neutrons were counted by a two-dimensional (2D) position-sensitive detector located at 20 m downstream of the sample. The neutron

wavelength was set to 10 Å. To measure the SANS pattern for the beam along the *c* axis, twenty-seven pieces of crystals, of the total volume of 4.6 mm^3, were aligned on an aluminum plate by their (001) crystal surface and in-plane orientation co-aligned by X-ray diffraction. To maximize the signal to background ratio a boron-carbide mask was mounted directly on the sample holding Al-plate around the sample. The sample on the Al-plate was mounted into a ^{3}He-circulation refrigerator with its (001) direction parallel to the incident beam. The precision of the temperature is better than ± 0.01 K during each integration time. For the case of the field-scan measurement under *H*//*a* (Figs. 1(e)-1(f) and Figs. S2(a)-S2(e)), the temperature gradually increases from 6.18 K (Fig. 1(e)) to 6.27 K (Fig. 1(f)), where the temperature fluctuation for each measurement is 0.003 K on average and 0.009 K in maximum. The incident beam was narrowed by the built-in diaphragm to the co-aligned-crystals sample area of 6×4 mm^2 on the sample. A magnetic field along or perpendicular to the incident beam was generated by an electro-magnet. To avoid the effect of the residual field, the electromagnet was demagnetized before performing the zero and subsequent applied field experiments. Background was measured in the field-polarized state of the sample and subtracted from the SANS patterns.

Figures S2(a)-S2(e) show the field-evolution of the SANS pattern for the co-aligned single crystals under *H*//*a* (see Fig. S2(e) for the direction of *H*). The neutron beam is parallel to the *c* axis. Four-fold pattern in zero field (Fig. S2(a)) indicates the multidomain state of the single-*q* cycloidal spin order. On the other hand for $H = 120$ Oe (Fig. S2(e)), no magnetic scattering is discerned due to entering the field-forced ferrimagnetic state as shown in Fig. 1(d). Prior to the transition to ferrimagnetic state,

we observed that the vertical spots for $\vec{q} \parallel \vec{a}$ rapidly disappear as the field increases while the intensity of the horizontal spots for $\vec{q} \parallel \vec{b}$ remains. The two-fold pattern for H = 80 Oe in Fig. S2(d) indicates that the single domain state of the single-q cycloidal spin state is selected.

This field-induced domain rearrangement is consistent with the hysteresis of magnetic property under $H//a$. Figures S2(f)-S2(g) show the H dependence of magnetic susceptibility χ' and the integrated intensities, I_v and I_h, for the vertical and horizontal sectors, respectively. The integration region for each component is shown as the inset in Fig. S2(g). The hysteresis for χ' closes at around 20 Oe, which is consistent with the disappearance of the I_v in the H-increasing process. The I_v does not recovered when H goes back to the zero field from 120 Oe, while the I_h slightly gains as compared to the initial value. This corresponds to the two-fold pattern shown in Fig. 1(f), in which a single-q domain in $q \perp H$ condition is selected by the field-trained process.

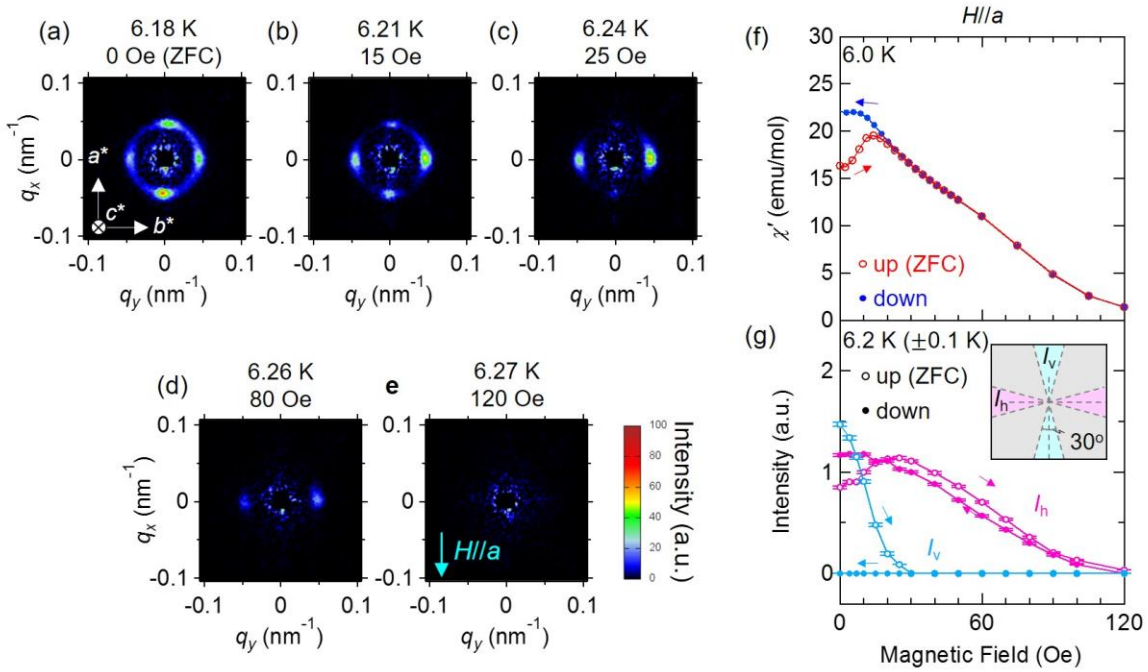

FIG. S2. (a-e) Magnetic-field (H) induced evolution of the SANS pattern for the co-aligned single crystals under $H//a$. The direction of H is indicated in (e). The measurement was performed in the H-increasing process at 6.2 K ($\pm$0.1 K). During the measurement, the temperature gradually increases from 6.18 K (Fig. 1(e)) to 6.27 K (Fig. 1(f)), where the temperature fluctuation for each measurement is 0.003 K on average and 0.009 K in maximum. Prior to the measurement, the sample was cooled down in zero field from the paramagnetic region. (f,g) H dependence of (f) the real part of the ac magnetic susceptibility χ', and (g) the integrated SANS intensities, I_v (blue circle) and I_h (pink circle), involving the Bragg reflections for the vertical and the horizontal region, respectively. The integration regions for I_v and I_h are the blue and pink region, respectively, as shown in the inset. The measurement was performed after the zero-field cooling process followed by the H-increasing scan (open circle), and then H-decreasing scan (closed circle).